Electronic Supplementary Material (ESI) for Physical Chemistry Chemical Physics.

Supporting Information

Photoelectrochemical OER activity by employing $BiVO_4$ with manganese oxide co-catalysts

Manjodh Kaur, Manjeet Chhetri and C. N. R. Rao*

New Chemistry Unit, International Centre for Materials Science, School of Advanced Materials and Sheikh Saqr Laboratory, Jawaharlal Nehru Centre for Advanced Scientific Research, Jakkur P.O., Bangalore 560064, India

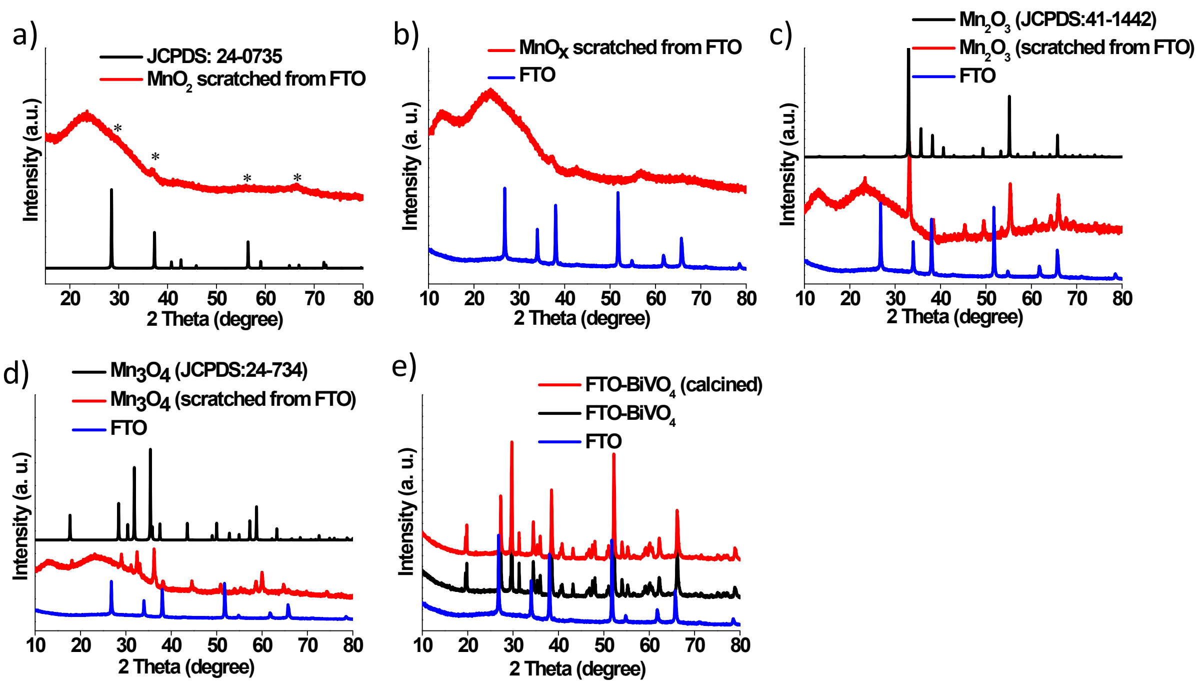

Fig. S1. Powder X-ray diffraction matched with ICDD files for a) MnO_2 b) MnO_x, for comparison FTO pattern is shown as the powder was deposited and scratched from FTO and highlights the absence of scratched SnO_2 c) Mn_2O_3 d) Mn_3O_4 e) FTO-$BiVO_4$ was heated at 600 ^{o}C and no change in the diffraction pattern was observed in comparison to the unannealed FTO-$BiVO_4$.

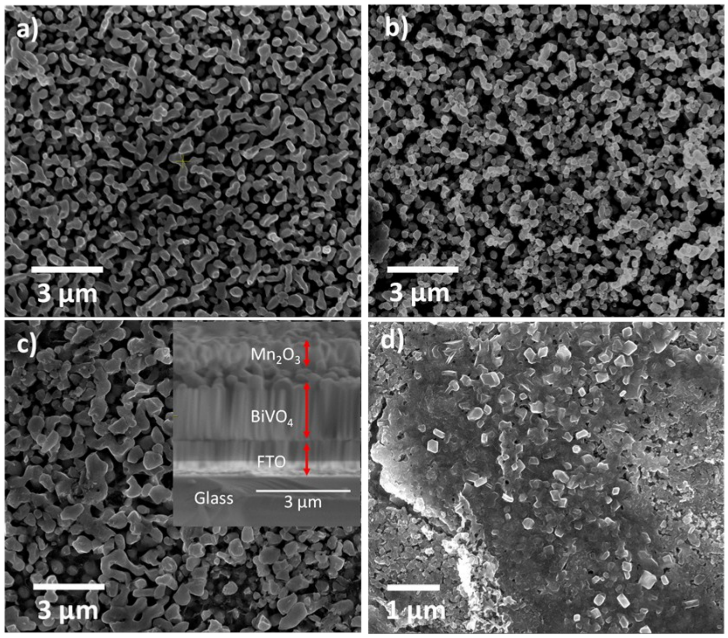

Fig. S2. FESEM top view of the electrode for a) FTO-$BiVO_4$ b) FTO-$BiVO_4$-MnO_2 c) FTO-$BiVO_4$-Mn_2O_3 (inset image showing cross-section of FTO-$BiVO_4$-Mn_2O_3 showing the electrodeposition of different layers d) FTO-$BiVO_4$-Mn_3O_4.

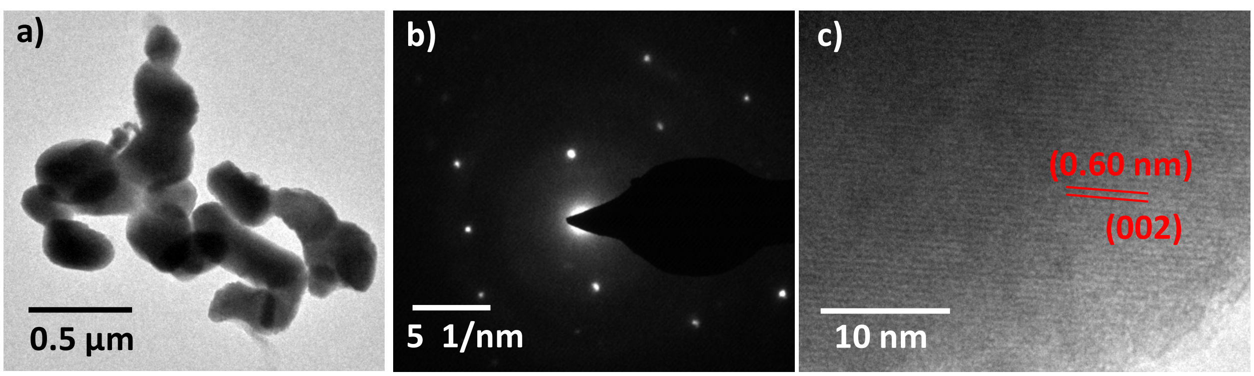

Fig. S3. a) TEM images for $BiVO_4$ scratched from FTO b) SAED pattern showing the crystalline nature of the $BiVO_4$ c) HRTEM image of $BiVO_4$ showing lattice fringe for the plane (002).

Note: Transmission electron microscopy (TEM) of $BiVO_4$ has shown the presence of particles of size range 0.5-1 µm. Small area electron diffraction (**Fig. S3b**) signifies the crystalline nature and HRTEM (**Fig. S3c**) reveals the presence of lattice fringes corresponding to the plane (002).

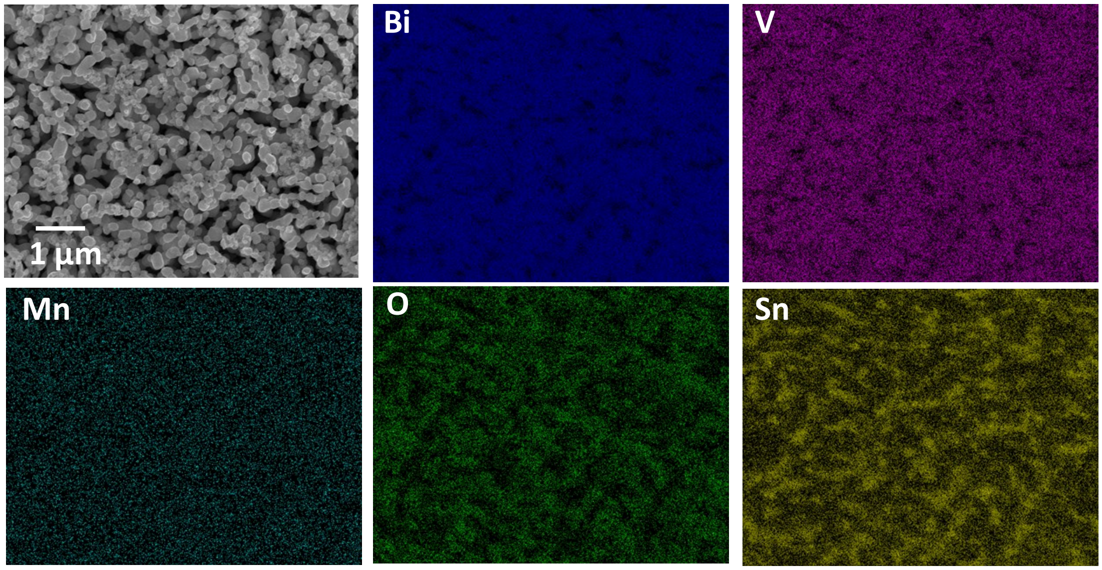

Fig. S4. Elemental mapping of top surface of FTO-$BiVO_4$-MnO_x showing uniform distribution of elements Bi, V, Sn, Mn, O and C.

Note: Elemental mapping of top view of FTO-$BiVO_4$-MnO_x studies show has highlighted the uniform distribution of the Bi, V, Mn, O, C and Sn elements on the electrode surface.

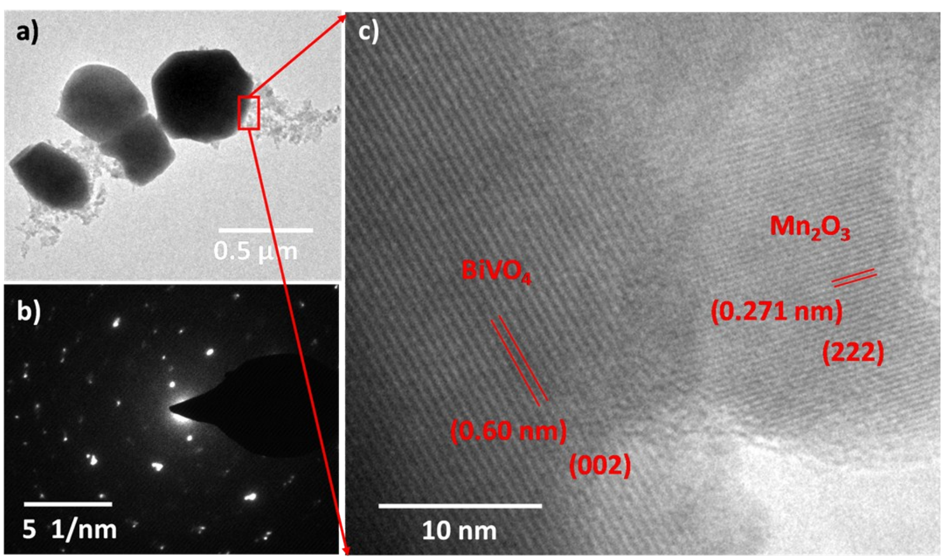

Fig S5. a) TEM images for $BiVO_4$-Mn_2O_3 scratched from FTO b) SAED pattern showing the crystalline nature of the $BiVO_4$ depicted by big spots and small spots correspond to Mn_2O_3 c) HRTEM image of $BiVO_4$ showing lattice fringe in close proximity of lattice fringe of Mn_2O_3 and their respective lattice fringes with interplanar spacing of 0.60 nm (002) and 0.27 nm (222) for $BiVO_4$ and Mn_2O_3 respectively.

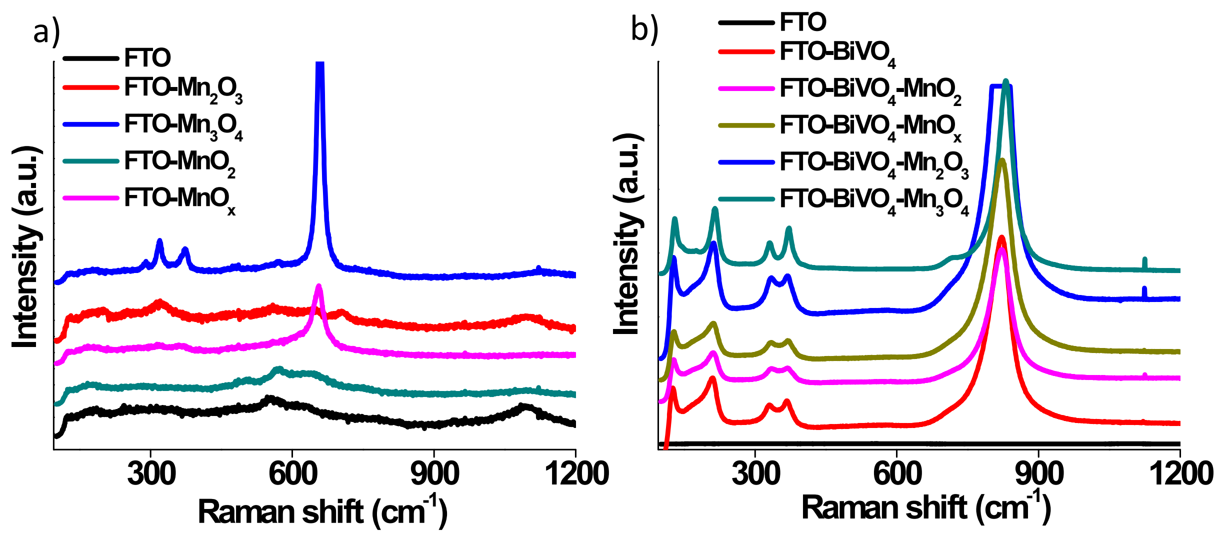

Fig S6. Raman analyses for a) deposited Manganese oxides on FTO b) deposited Manganese oxides on FTO-$BiVO_4$.

Note: Raman analyses (**Fig. S6a**) for MnO_2 shows weak peaks at 503, 570, 644 and 756 cm^{-1}, raman modes at 570 cm^{-1} and 644 cm^{-1} corresponds to the A_g breathing vibrations of MnO_6 octahedra in the structure.[1] Raman analysis of Mn_2O_3 (**Fig. S6a**) depicts peaks at 321, 559, 650 and 707 cm^{-1} corresponds to the vibrational modes corresponding to out of plane symmetric and asymmetric vibrations of Mn-O-Mn species.[2] In the case of Mn_3O_4 (**Fig. S6a**) characteristic band is observed at 655 cm^{-1} in addition to other vibration modes at 289, 321, 372, 483, 572 cm^{-1}. The band at 655 cm^{-1} corresponds to A_{1g} mode of vibration of Mn-O breathing vibrations of Mn^{2+} in tetrahedral coordination which supports the presence of Mn_3O_4 phase of Mn oxide.[3] Mn_3O_4 is obtained by heat treatment at 600 ^oC from the MnO_2. The heat treatment helps in the intercalation of Mn^{2+} ions in the tetrahedral sites and results in phase transformation of MnO_2 to Mn_3O_4.[4] Whereas, the Raman spectra of MnO_x (**Fig. S6a**) shows vibration modes at 321, 650 and 707 cm^{-1} which are matching with the peak both from the Mn_2O_3 and Mn_3O_4 and clearly signifies the mixed phase nature of the material i.e. a combination of Mn^{3+} and Mn^{4+} oxidation states. Typical vibrations corresponding to the $BiVO_4$ are observed at 129, 210, 330, 366, 702 and 820 cm^{-1} as shown in **Fig. S6b**. Bands at 330 and 366 cm^{-1} depict the asymmetric and symmetric formations of VO_4 tetrahedron. Raman bands centred at 702 and 820 cm^{-1} indicate the two vibrational modes of V-O bonds. With addition of Mn oxides and annealing at different temperatures, shift in the peaks of electrodeposited $BiVO_4$ is observed due to the change in the electronic environment by electrodeposition of the Mn oxides.[5] The peaks corresponding to different Mn oxides on the $BiVO_4$ were not observed clearly in **Fig. S6b** due to high intensity signals of $BiVO_4$ due to lesser deposition of respective Mn oxides.

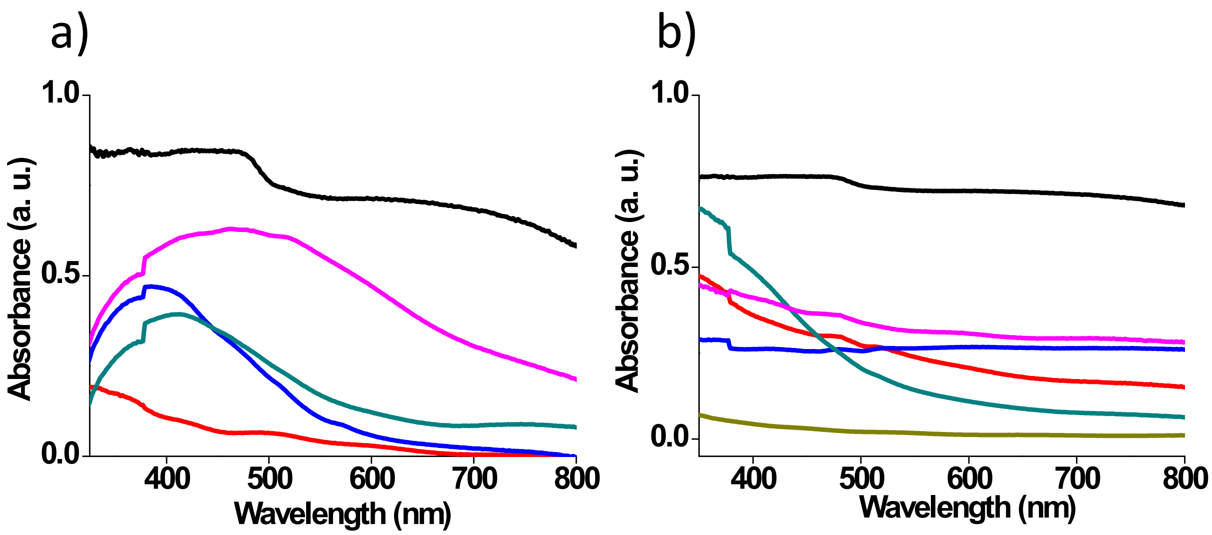

Fig. S7. a) UV-vis absorption spectra of electrodeposited Mn oxides, FTO-$BiVO_4$ (black line), FTO-MnO_2 (green line), FTO-MnO_x (pink line), FTO-Mn_2O_3 (red line), FTO-Mn_3O_4 (blue line) b) UV-vis absorption spectra of electrodeposited Mn oxides on FTO-$BiVO_4$ (black line), FTO-$BiVO_4$-MnO_2 (green), FTO-$BiVO_4$-MnO_x (pink), FTO-$BiVO_4$-Mn_2O_3 (red), FTO-$BiVO_4$-Mn_3O_4 (blue).

Note: FTO-MnO_x showed broad absorption edge highlighting the presence of mixture of oxides in its composition. FTO-MnO_2 shows broad absorption edge in the range of 411-560 nm owing to the possible d-d transitions in the lower t_{2g} and higher e_g energy levels in the ligand field of MnO_6 octahedra.[6] FTO-Mn_2O_3 has shown absorption edges at 360, 423 and 512 nm. Absorption at 360 nm is the characteristic of the presence of Mn^{+3} ions in the sample.[7] Broad absorption peaks are observed at 417, 510 and 571 nm for FTO-Mn_3O_4 relating to the Jahn–Teller (J–T) distorted d-d transitions possible in the structure and band gap plots are shown in **Fig. S7a**.[8] The absorption spectra of deposition of Mn oxides on the FTO-$BiVO_4$ were recorded (**Fig. S7b**). The absorption spectra of the films showed broad absorption range of 443-668 nm and 452-648 nm in the case of FTO-$BiVO_4$-MnO_x and FTO-$BiVO_4$-Mn_2O_3 respectively. This indicated that the photoanodes are suitable for visible light absorption and have the required band gaps of 2.5-2.6 eV as shown in **Fig. S7**. A sharp fall in the absorbance was obtained in the range of 400-518 nm for FTO-$BiVO_4$-MnO_2 corresponding to the band gap of 2.49 eV. Band gap of 2.25 eV was obtained for FTO-$BiVO_4$-Mn_3O_4 owing to the weak absorption edges at 413, 484 and 604 nm. Band gap plots have been shown on **Figure S8, S9** and the values are tabulated in **Table S1**. Band gaps have been calculated using the Tauc plots using the relation:

$$\alpha h\nu = A\,(h\nu - E_g)^n$$

where, α is the absorption coefficient (cm^{-1}), hν is the photon energy (eV), A is the constant, E_g is the band gap (eV) and n determines the type of transition and has value ½, 3/2, 2 and 3 for direct allowed, direct forbidden transition, indirect allowed and indirect forbidden transition, respectively.

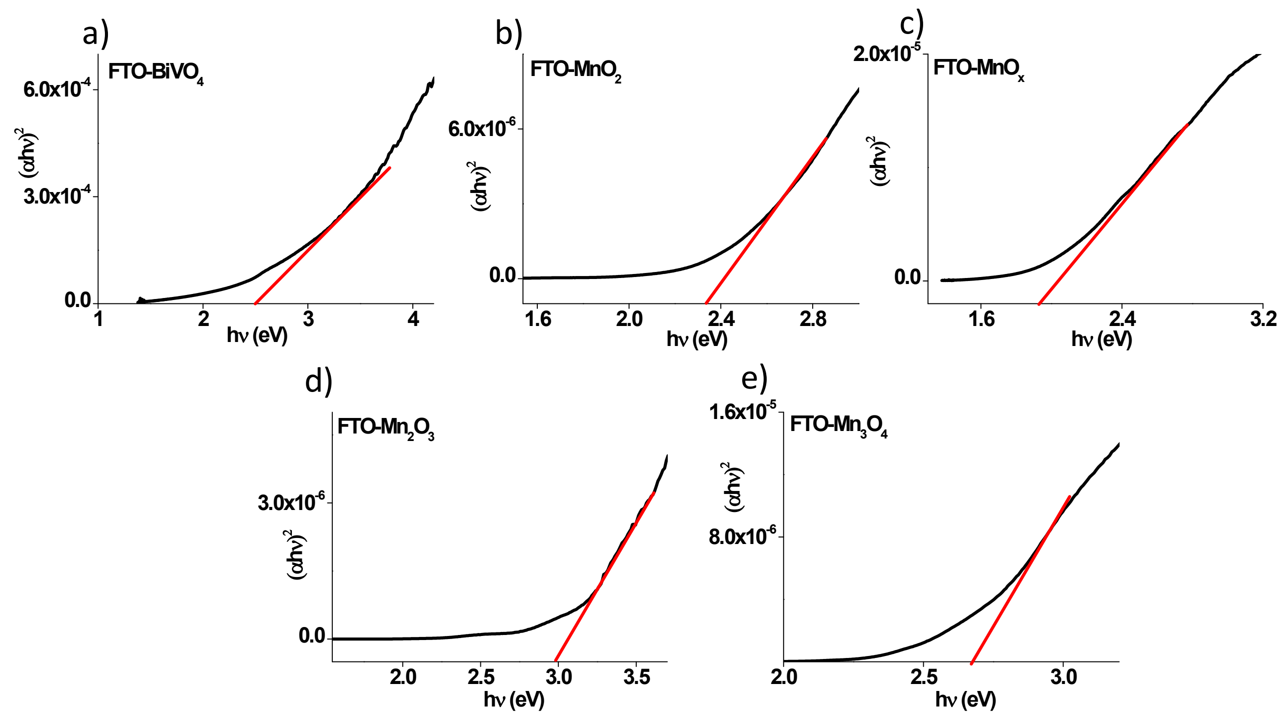

Fig. S8. Band gap plots from Tauc relations are shown for a) FTO-$BiVO_4$ b) FTO-MnO_2 c) FTO-MnO_x d) FTO-Mn_2O_3 e) FTO-Mn_3O_4.

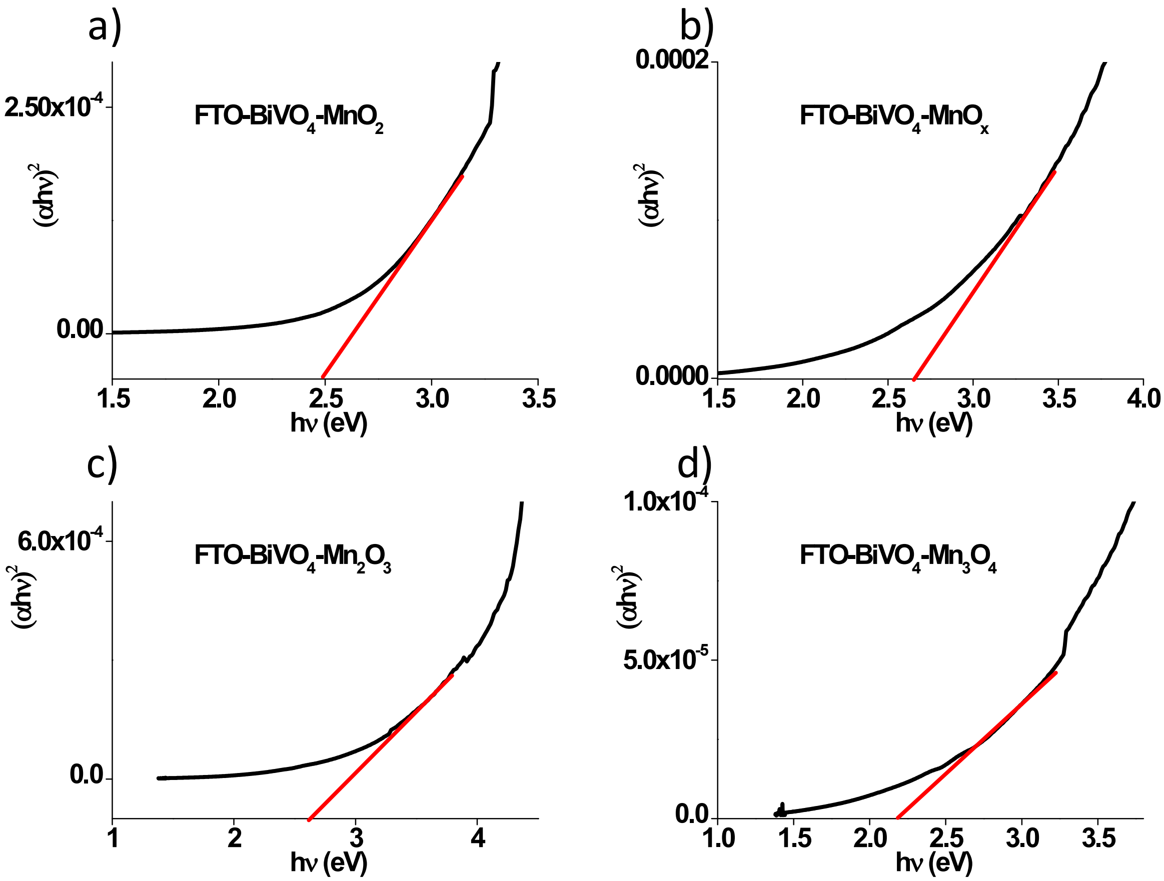

Fig. S9. Band gap plots from Tauc relations are shown for a) FTO-$BiVO_4$-MnO_2 b) FTO-$BiVO_4$-MnO_x c) FTO-$BiVO_4$-Mn_2O_3 d) FTO-$BiVO_4$-Mn_3O_4.

Table S1. Band gap values obtained from Tauc plot:

Compound	Band Gaps from Tauc plots (eV)
FTO-$BiVO_4$	2.64
FTO-MnO_2	2.34
FTO-Mn_2O_3	2.99
FTO-MnO_x	1.87
FTO-Mn_3O_4	2.63
FTO-$BiVO_4$-MnO_2	2.49
FTO-$BiVO_4$-Mn_2O_3	2.51
FTO-$BiVO_4$-MnO_x	2.65
FTO-$BiVO_4$-Mn_3O_4	2.25

Table S2. XPS deconvoluted peaks for Mn and Bi summarised:

Compound	Mn2p (eV)		Bi4f (eV)	
	$2p_{3/2}$	$2p_{1/2}$	4f7/2	4f5/2
FTO-$BiVO_4$	-	-	158.58	163.84
FTO-$BiVO_4$-MnO_2	642.90	654.43	159.07	164.33
FTO-$BiVO_4$-MnO_x-before PEC	641.52/644	653.42	158.61	163.96
FTO-$BiVO_4$-MnO_x-after PEC	641.52/643.45	654.16	159.12	164.40
FTO-$BiVO_4$-Mn_2O_3	641.60	653.17	157.92	163.20
FTO-$BiVO_4$-Mn_3O_4	639.03/641.98	653.12	158.64	163.93

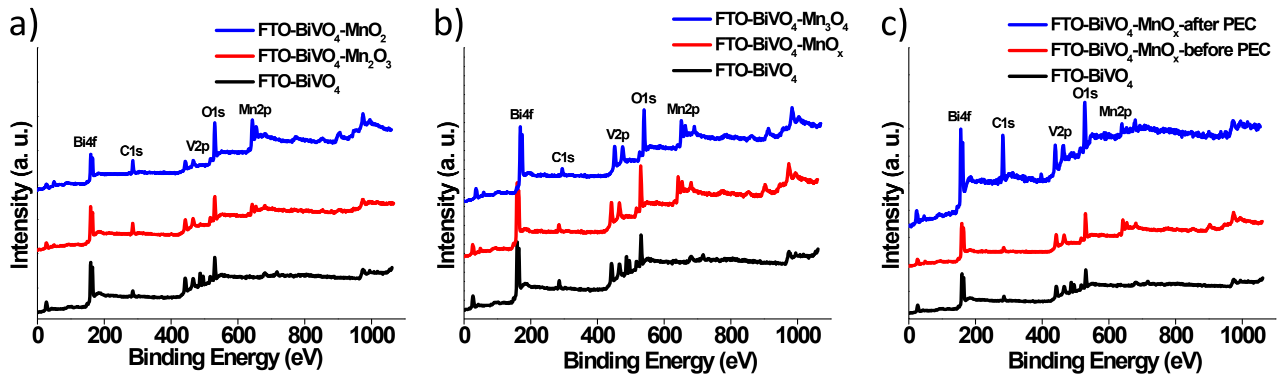

Fig. S10. X-ray photoelectron survey scan spectra for a)FTO-$BiVO_4$, FTO-$BiVO_4$-MnO_2 and FTO-$BiVO_4$-Mn_2O_3 b) FTO-$BiVO_4$, FTO-$BiVO_4$-MnO_x and FTO-$BiVO_4$-Mn_3O_4 c) FTO-$BiVO_4$, FTO-$BiVO_4$-MnO_x before Photoelectrochemical water splitting (PEC) and FTO-$BiVO_4$-MnO_x after PEC.

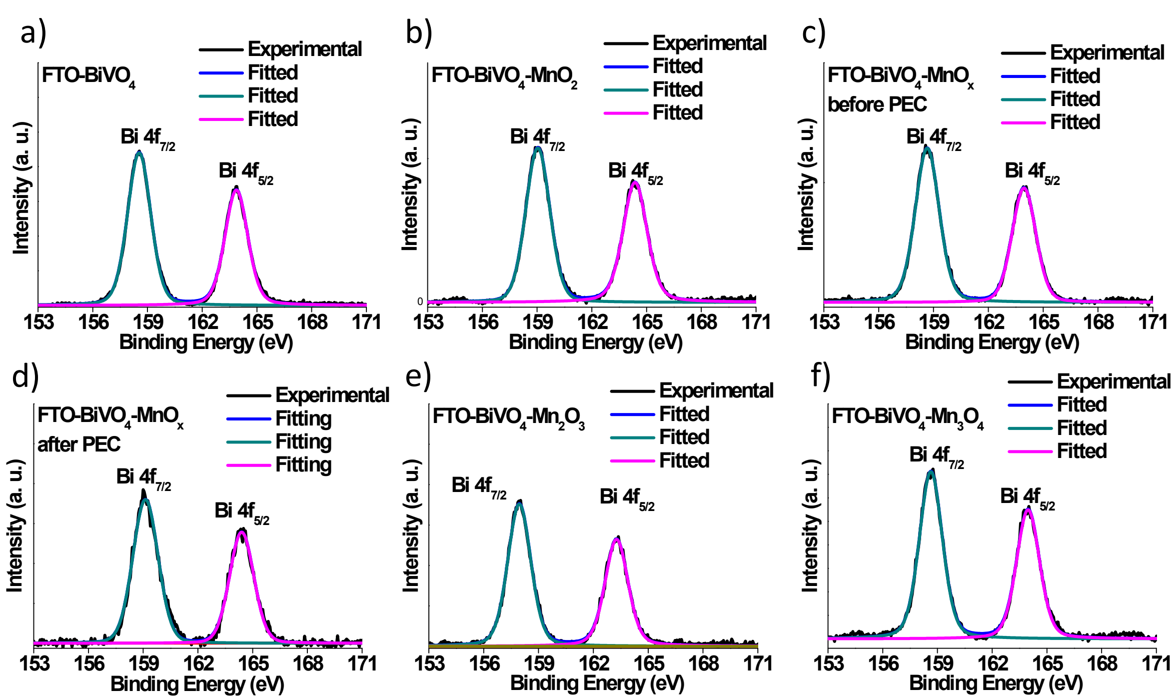

Fig. S11. Deconvoluted peaks of Bi $4f_{7/2}$ and Bi $4f_{5/2}$ for a) FTO-$BiVO_4$ b) FTO-$BiVO_4$-MnO_2 c) FTO-$BiVO_4$-MnO_x before Photoelectrochemical water splitting (PEC) d) FTO-$BiVO_4$-MnO_x after PEC e) FTO-$BiVO_4$-Mn_2O_3 f) FTO-$BiVO_4$-Mn_3O_4.

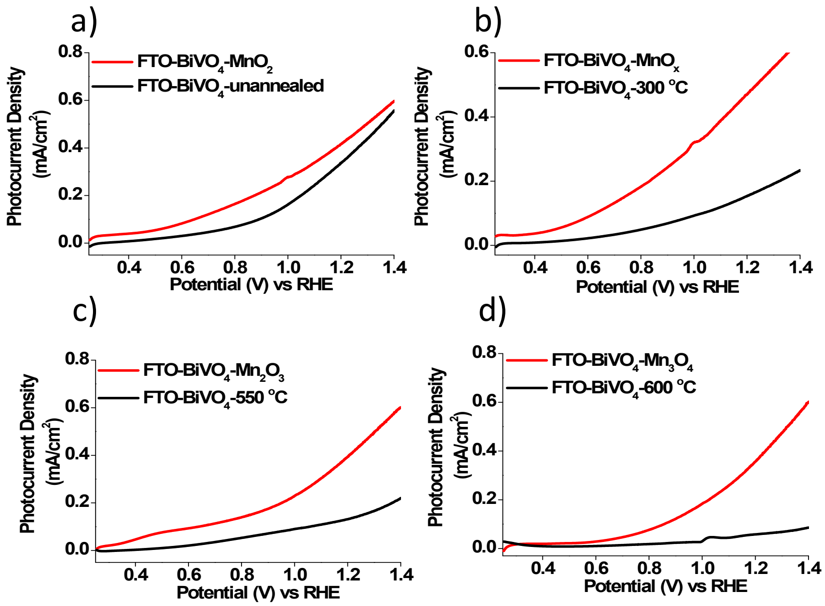

Fig. S12. Photocurrent density (J) vs Potential (V) vs RHE curves for full light illumination for a) FTO-$BiVO_4$-MnO_2 compared with unannealed $BiVO_4$ b) FTO-$BiVO_4$-MnO_x compared with $BiVO_4$ annealed at 300 ^oC c) FTO-$BiVO_4$-Mn_2O_3 compared with $BiVO_4$ annealed at 550 ^oC d) FTO-$BiVO_4$-Mn_3O_4 compared with $BiVO_4$ annealed at 600 ^oC under visible light illumination of 100 mW/cm^2 in 0.1 M Potassium phosphate (KPi) buffer solution (pH=7).

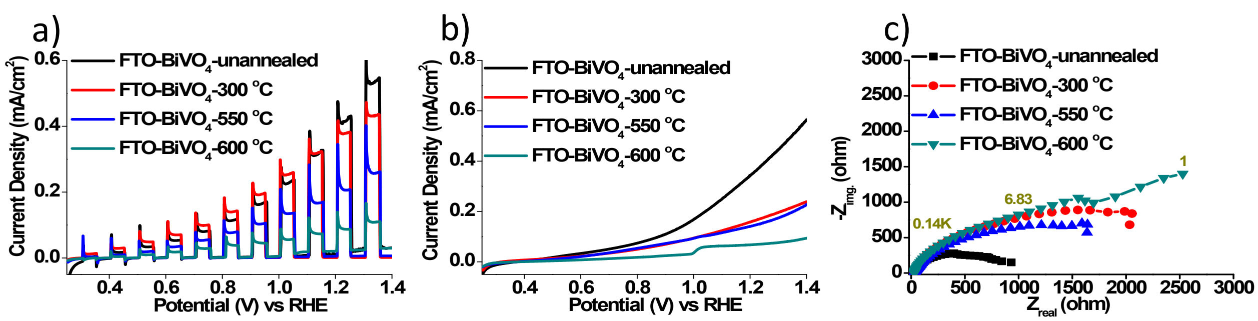

Fig. S13. a) Comparison of J-V curves for chopped light illumination for FTO-$BiVO_4$ unannealed with the FTO-$BiVO_4$ annealed at 300 ^oC, 550 ^oC and 600 ^oC b) Comparison of J-V curves for full light illumination for FTO-$BiVO_4$ unannealed with the FTO-$BiVO_4$ annealed at 300 ^oC, 550 ^oC and 600 ^oC c) Comparison of Nyquist plots of FTO-$BiVO_4$ unannealed with the FTO-$BiVO_4$ annealed at 300 ^oC, 550 ^oC and 600 ^oC, the numerical values (dark yellow font) in the plots represent the respective frequencies of the three data points below them, under visible light illumination of 100 mW/cm^2 in 0.1 M Potassium phosphate (KPi) buffer solution (pH=7).

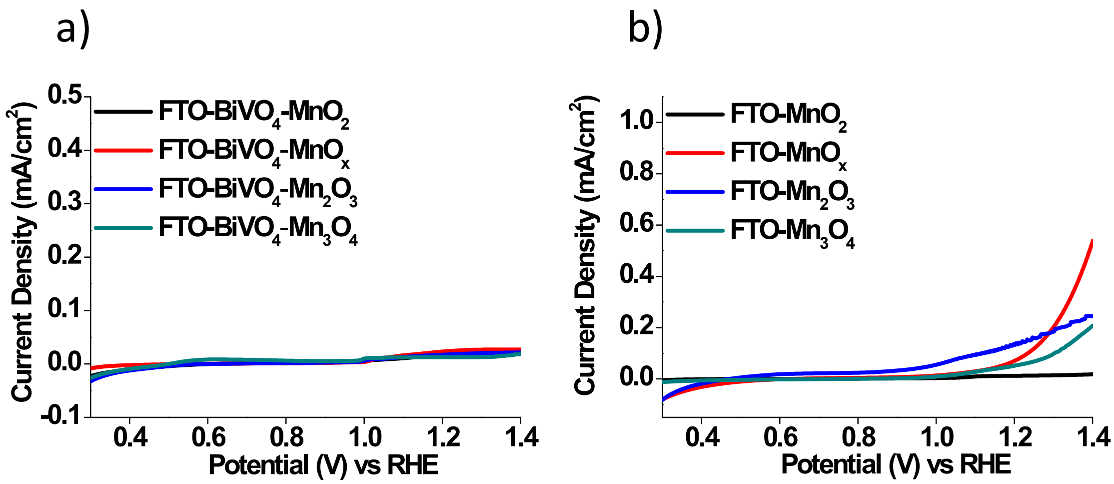

Fig. S14. Current density (J) vs Potential (V) vs RHE curves for a) FTO-BiVO$_4$-MnO$_{2,}$ FTO-BiVO$_4$-MnO$_x$, FTO-BiVO$_4$-Mn2O3 and FTO-BiVO$_4$-Mn$_3$O$_4$ in dark in 0.1 M Potassium phosphate (KPi) buffer solution (pH=7) b) in full light illumination for FTO-MnO$_2$, FTO-MnO$_x$, FTO-Mn$_2$O$_3$ and FTO-Mn$_3$O$_4$ in 0.1 M Potassium phosphate (KPi) buffer solution (pH=7).

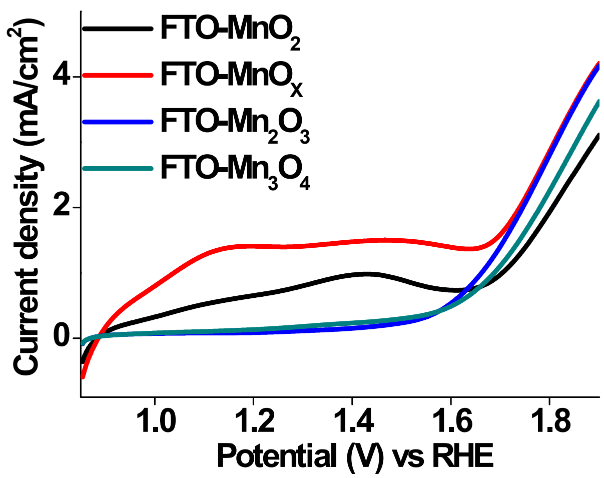

Fig. S15. Comparison of Current Density (J) as a function of potential (V) vs RHE of FTO-MnO$_2$, FTO-MnO$_x$, FTO-Mn$_2$O$_3$, FTO-Mn$_3$O$_4$ in 0.1 M Potassium phosphate (KPi) buffer solution (pH=7).

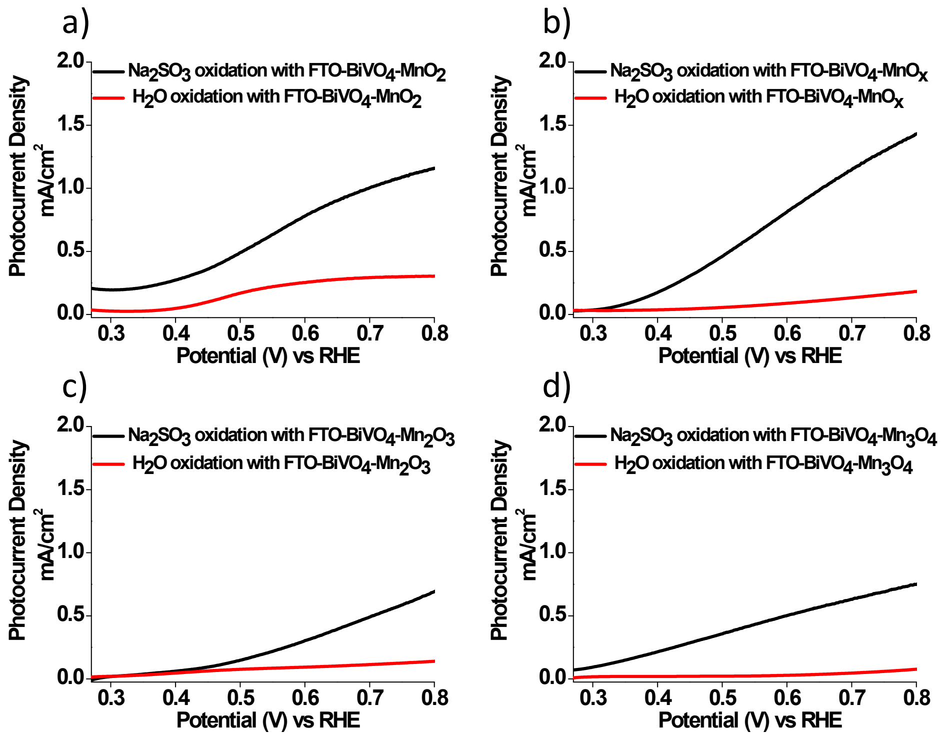

Fig. S16. Photocurrent density (J) vs Potential (V) (vs RHE) plots for Na_2SO_3 vs H_2O oxidation for a) FTO-$BiVO_4$-MnO_2 b) FTO-$BiVO_4$-MnO_x c) FTO-$BiVO_4$-Mn_2O_3 d) FTO-$BiVO_4$-Mn_3O_4 under visible light illumination of 100 mW/cm^2 in 0.1 M Potassium phosphate (KPi) buffer solution (pH=7).

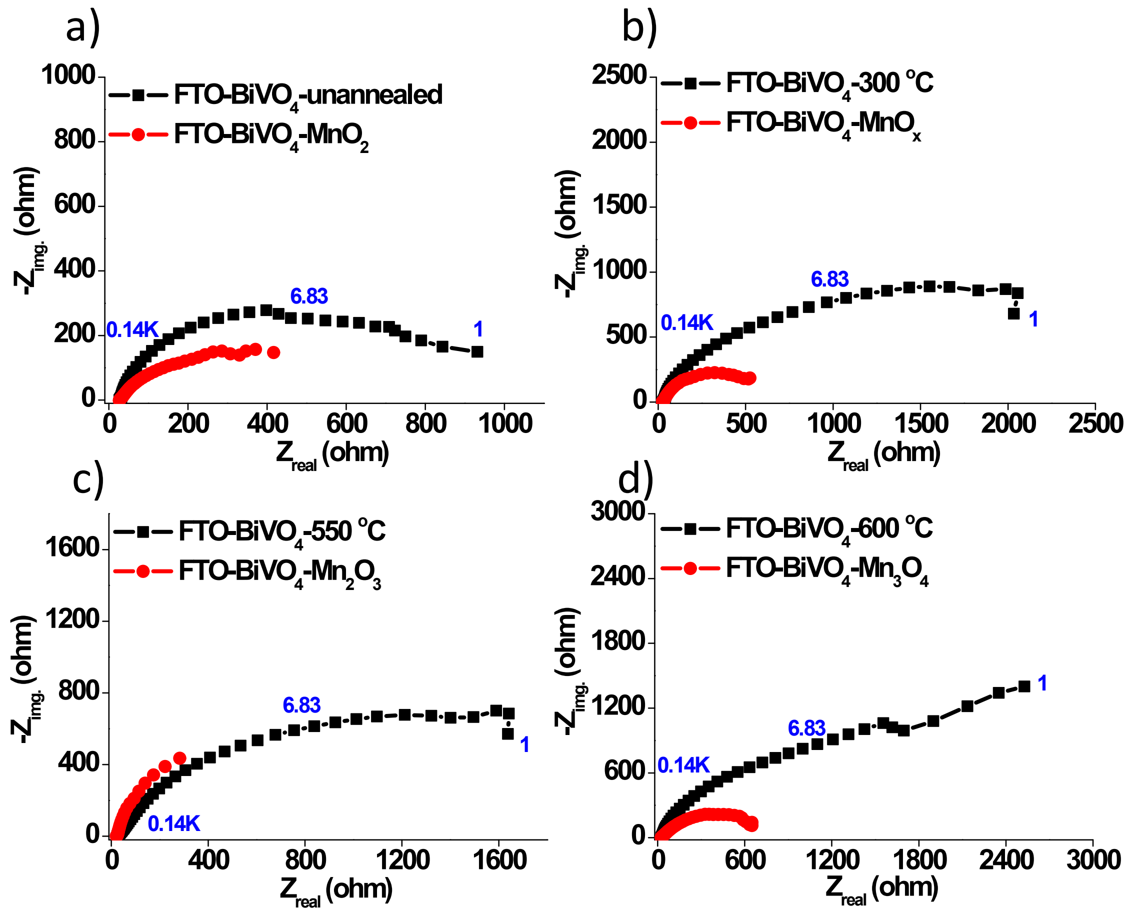

Fig. S17. Nyquist plots in full light illumination for a) FTO-$BiVO_4$-MnO_2 compared with unannealed $BiVO_4$ b) FTO-$BiVO_4$-MnO_x compared with $BiVO_4$ annealed at 300 ^oC c) FTO-$BiVO_4$-Mn_2O_3 compared with $BiVO_4$ annealed at 550 ^oC d) FTO-$BiVO_4$-Mn_3O_4 compared with $BiVO_4$ annealed at 600 ^oC under visible light illumination of 100 mW/cm^2 in 0.1 M Potassium phosphate (KPi) buffer solution (pH=7), the numerical values (blue font) in the plots represent the respective frequencies of the three data points above/below them.

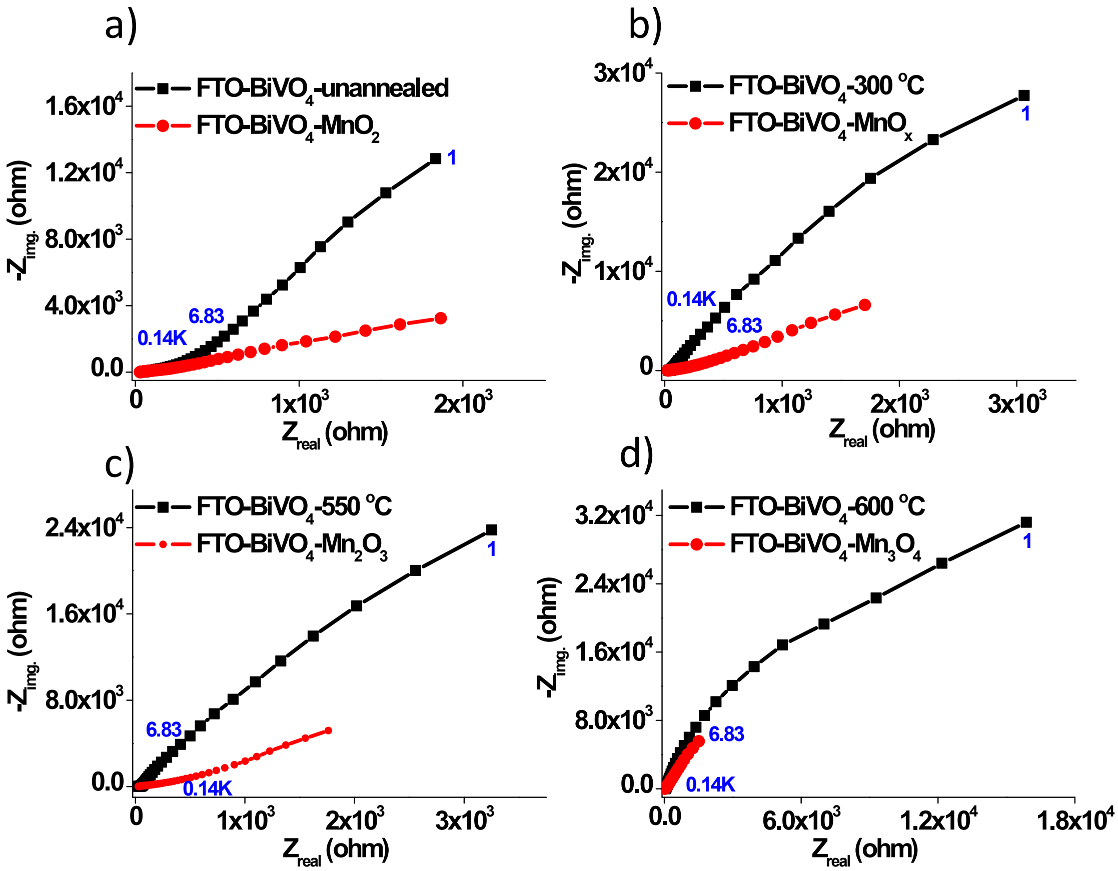

Fig. S18. Nyquist plots in dark for e) FTO-$BiVO_4$-MnO_2 compared with unannealed $BiVO_4$ f) FTO-$BiVO_4$-MnO_x compared with $BiVO_4$ annealed at 300 ^oC g) FTO-$BiVO_4$-Mn_2O_3 compared with $BiVO_4$ annealed at 550 ^oC h) FTO-$BiVO_4$-Mn_3O_4 compared with $BiVO_4$ annealed at 600 ^oC in 0.1 M Potassium phosphate (KPi) buffer solution (pH=7), the numerical values (blue font) in the plots represent the respective frequencies of the three data points above/below them.

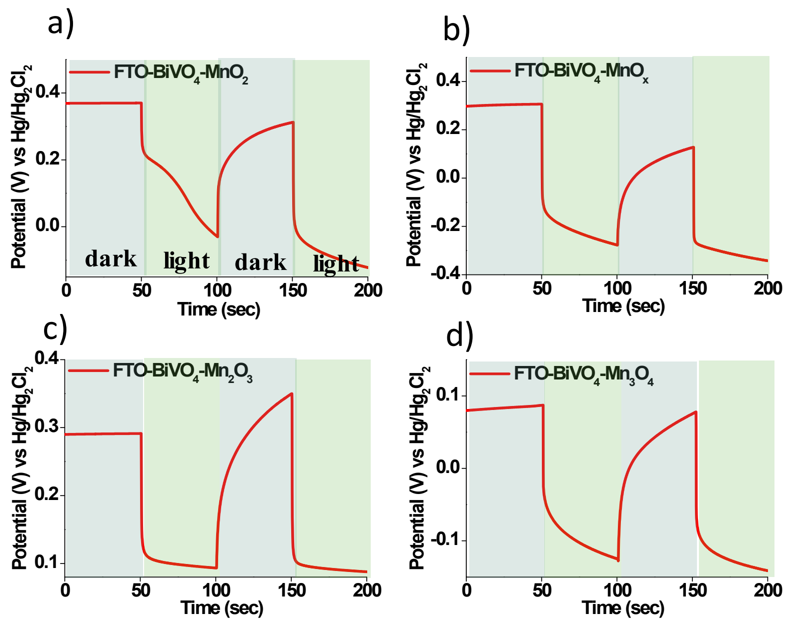

Fig. S19. Open circuit potential (ocp) vs time plots for consecutive light and dark illumination for c) FTO-$BiVO_4$-MnO_2 d) FTO-$BiVO_4$-MnO_x e) FTO-$BiVO_4$-Mn_2O_3 f) FTO-$BiVO_4$-Mn_3O_4 under visible light illumination of 100 mW/cm^2 in 0.1 M Potassium phosphate (KPi) buffer solution (pH=7).

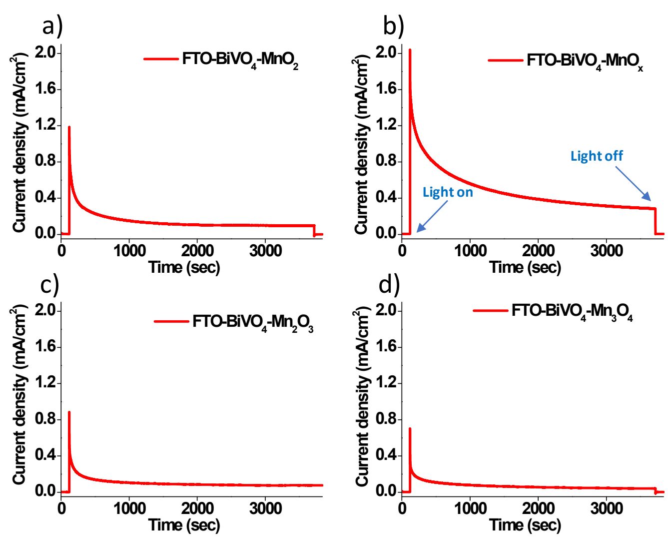

Fig. S20. Current Density (J) vs t plots showing stability of a) FTO-$BiVO_4$-MnO_2 b) FTO-$BiVO_4$-MnO_x c) FTO-$BiVO_4$-Mn_2O_3 d) FTO-$BiVO_4$-Mn_3O_4 under visible light illumination of 100 mW/cm^2 in 0.1 M Potassium phosphate (KPi) buffer solution (pH=7). Light was switched on 120 sec after illumination and switched off 120 sec before the analysis time is over.

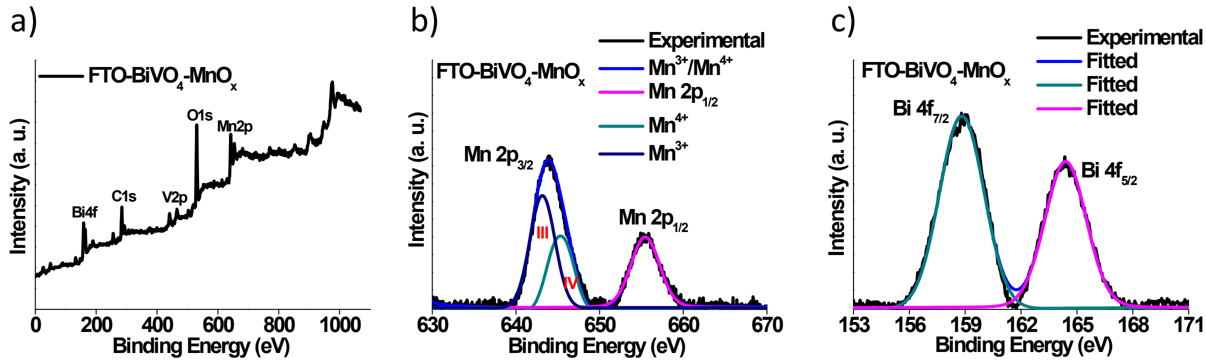

Fig. S21. X-ray photoelectron spectra for FTO-$BiVO_4$-MnO_x a) survey scan b) deconvoluted peaks of Mn $2p_{3/2}$ and Mn $2p_{1/2}$ c) deconvoluted peaks of of Bi $4f_{7/2}$ and Bi $4f_{5/2}$.

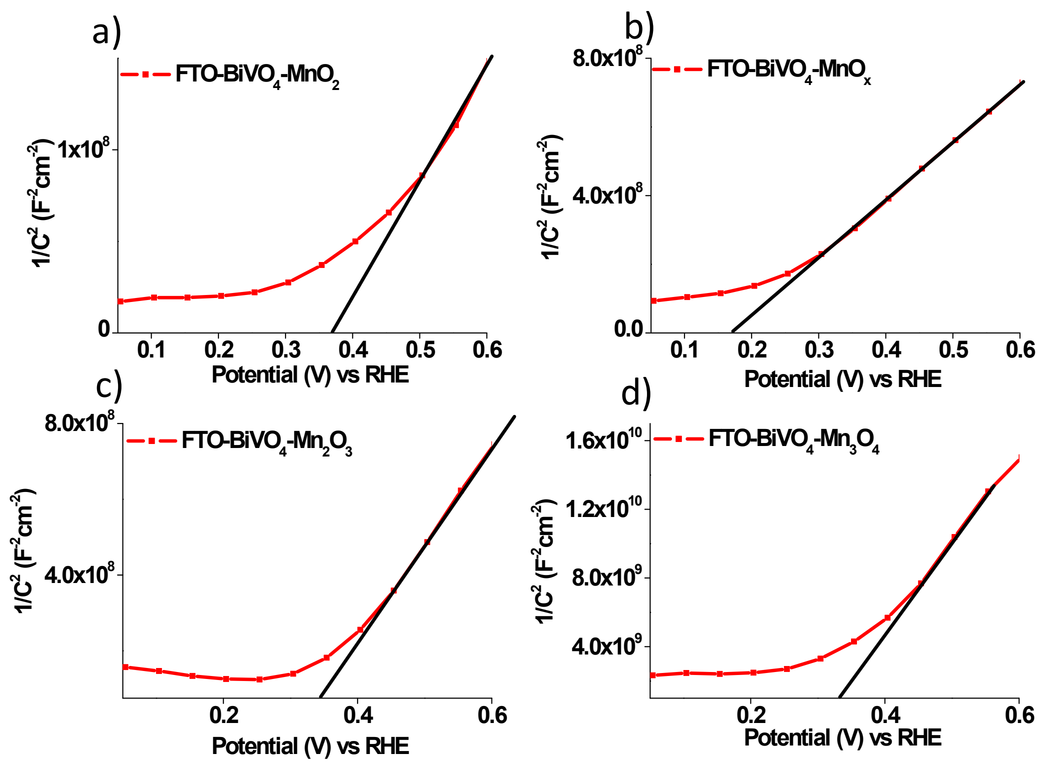

Fig. S22. Mott-Schottky plots for full light illumination for a) FTO-$BiVO_4$-MnO_2 b) FTO-$BiVO_4$-MnO_x c) FTO-$BiVO_4$-Mn_2O_3 d) FTO-$BiVO_4$-Mn_3O_4 under visible light illumination of 100 mW/cm^2 in 0.1 M Potassium phosphate (KPi) buffer solution (pH=7).

Table S3: Calculations for Flat band potential for photoanodes:

Photoelectrode	Intercept (V)	Flat band potential (V_{fb})
FTO-BiVO$_4$-MnO$_2$	**-2.36 x 10^8**	**0.34**
FTO-BiVO$_4$-MnO$_x$	**-2.89 x 10^8**	**0.14**
FTO-BiVO$_4$-Mn$_2$O$_3$	**-8.15 x 10^8**	**0.32**
FTO-BiVO$_4$-Mn$_3$O$_4$	**-1.66 x 10^{10}**	**0.30**

References

[1] T. Gaoa, H. Fjellvåga and P. Norby, *Analytica Chimica Acta*, 2009, **648**, 235.

[2] R. Naeem, M. A. Ehsan, R. Yahya, M. Sohail, H. Khaledic and M. Mazhar, *Dalton Trans*., 2016, **45**, 14928.

[3] C. Julien, M. Massot, C. Poinsignon, *Spectrochim. Acta Part A: Mol. Biomol.Spectrosc*., 2004, **60**, 689.

[4] S. Chenga, L. Yanga, D. Chenb , X. Jic , Z. Jianga , D. Dingb , M. Liu, *Nano Energy*, 2014, **9**, 161.

[5] S. R. M. Thalluri, C. Martinez-Suarez, A. Virga, N. Russo and G. Saracco, *Int. J.* ***Chem****. Eng*., 2013, **4**, 305.

[6] W. Li, X. Cui, R. Zeng, G. Du, Z. Sun, R. Zheng, S. P. Ringer and S. X. Dou, *Sci. Rep*., 2015, **5**, Article no. 8987.

[7] R. Naeem, M. A. Ehsan, R. Yahya, M. Sohail, H. Khaledic and M. Mazhar, *Dalton Trans*., 2016, **45**, 14928.

[8] a) H. Rahaman and S. K. Ghosh, *RSC Adv*., 2016, **6**, 4531 b) A. Giri, N. Goswami, C. Sasmal, N. Polley, D. Majumdar, S. Sarkar, S. N. Bandyopadhyay, A. Singhac and S. K. Pal, *RSC Adv*., 2014, **4**, 5075 c) A. Vazquez-olmos, R. Redon, A. L. Fernandez-osorio and J. M. Saniger, *Appl. Phys. A*, 2005, **81**, 1131.